Journal of Solid State Chemistry

Volume 200, Pages 1-362 (April 2013)

editorial board/cover legend

Page IFC

Table of Contents - Web Colour Only

Pages iii-xii

Regular Articles

Microporous metal organic framework [M_2(hfipbb)$_2$(ted)] (M=Zn, Co; H_2hfipbb=4,4-(hexafluoroisopropylidene)-bis(benzoic acid); ted=triethylenediamine): Synthesis, structure analysis, pore characterization, small gas adsorption and CO_2/N_2 separation properties

Original Research Article
Pages 1-6
William W. Xu, Sanhita Pramanik, Zhijuan Zhang, Thomas J. Emge, Jing Li

Graphical abstract

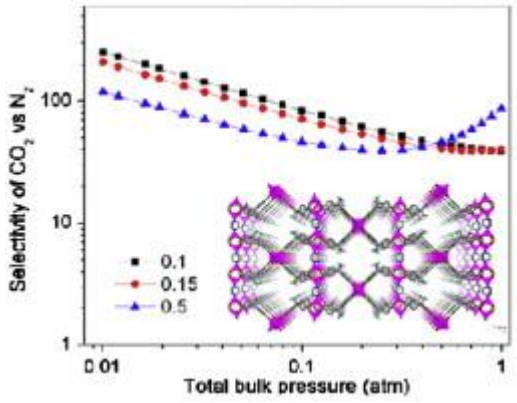

Highlights

► Two new porous MOFs were synthesized and characterized by rational design. ► The small pore size leads to greatly enhanced CO_2–MOF interaction. ► High adsorption selectivity of the Zn–MOF for CO_2 over N_2 is achieved.

Ce_2PdIn_8, Ce_3PdIn_{11} and $Ce_5Pd_2In_{19}$—members of homological series based on $AuCu_3$- and $PtHg_2$-type structural units

Original Research Article
Pages 7-12
A. Tursina, S. Nesterenko, Y. Seropegin, H. Noël, D. Kaczorowski

Graphical abstract

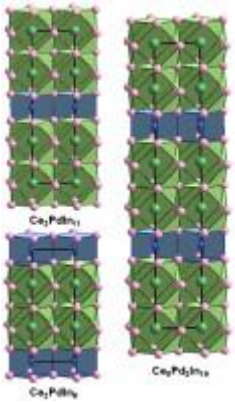

Highlights

► Large section of Ce–Pd–In phase diagram was examined. ► Three distinct ternary phases were identified, two of them for the first time. ► Crystal structures of two novel compounds constitute new structure types. ► The determined crystal structures show close mutual relationship. ► Ce_3PdIn_{11} and $Ce_5Pd_2In_{19}$ are paramagnetic Kondo lattices.

Molten salt flux synthesis and crystal structure of a new open-framework uranyl phosphate $Cs_3(UO_2)_2(PO_4)O_2$: Spectroscopic characterization and cationic mobility studies

Original Research Article
Pages 13-21
S. Yagoubi, C. Renard, F. Abraham, S. Obbade

Graphical abstract

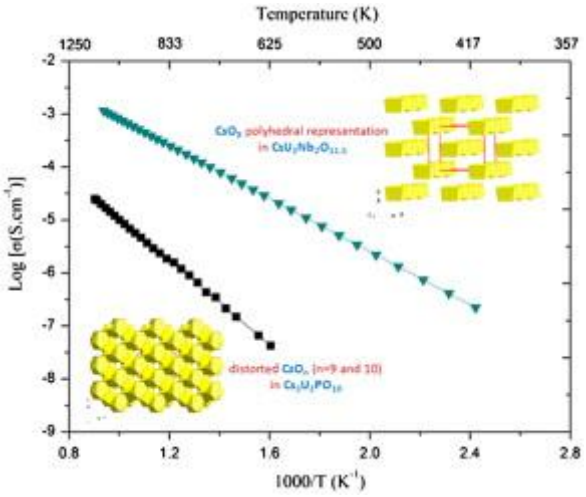

Highlights

► The reaction of $(UO_2)_3(PO_4)_2(H_2O)_4$ in excess of molten CsI leads to single-crystals of new tunneled compound $Cs_3(UO_2)_2(PO_4)O_2$. ► Ionic conductivity measurements and crystal structure analysis indicate a strong connection of the Cs^+ cations to the tunnels. ► A low symmetry in $Cs_3(UO_2)_2(PO_4)O_2$ is the cause of IR activation and splitting of the bands in the IR spectrum.

Structures and phases transition in hexylenediammonium pentachlorobismuthate (III) $[NH_3(CH_2)_6NH_3]BiCl_5$ crystal

Original Research Article
Pages 22-29
A. Ouasri, H. Jeghnou, A. Rhandour, P. Roussel

Graphical abstract

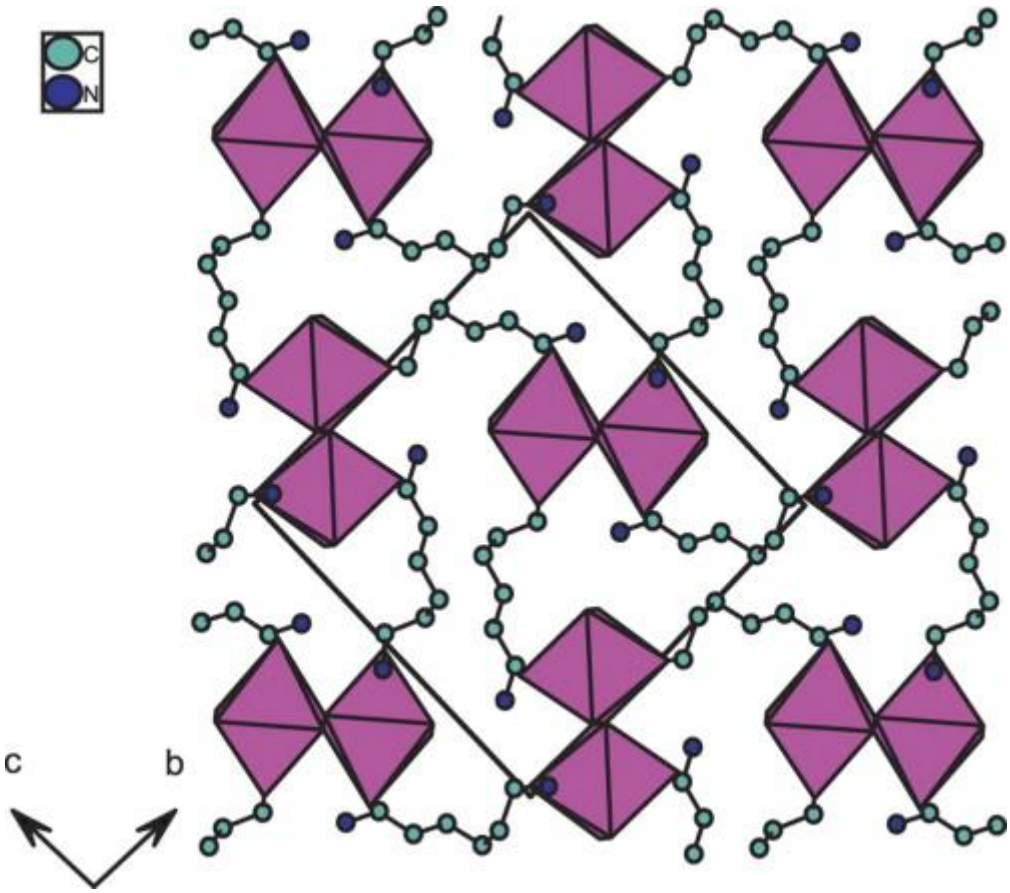

Highlights

► The crystal shows two phase transitions: α(223 K)↔β(308 K)↔γ(373 K). ► A discontinuous transition may be occurred between α and β phases. ► The α↔β and β↔γ phase transitions are of first order. ► Both anionic and cationic motions contribute to phase transition mechanisms. ► The $BiCl_6^{3-}$ octahedra showed significant distortions on decreasing temperature.

Synthesis and characterization of perovskite-type $Sr_xY_{1-x}FeO_{3-\delta}$ ($0.63 \leq x < 1.0$) and $Sr_{0.75}Y_{0.25}Fe_{1-y}M_yO_{3-\delta}$ (M=Cr, Mn, Ni), (y=0.2, 0.33, 0.5)

Original Research Article
Pages 30-38
J.J. Biendicho, S. Shafeie, L. Frenck, D. Gavrilova, S. Böhme, A.M. Bettanini, P. Svedlindh, S. Hull, Z. Zhao, S.Ya. Istomin, J. Grins, G. Svensson

Graphical abstract

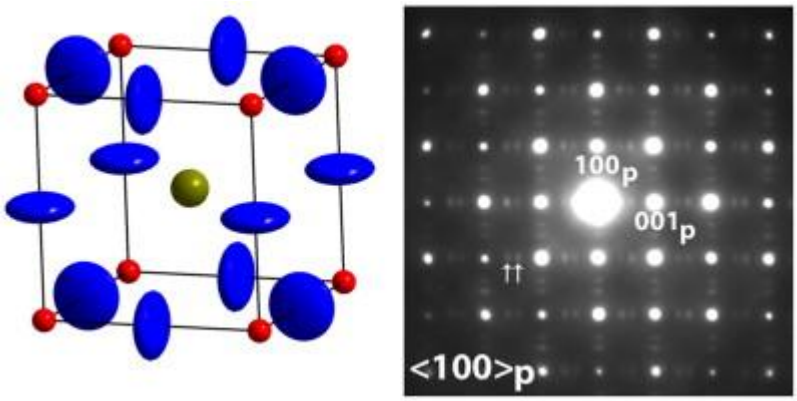

Highlights

► Cubic perovskites $Sr_xY_{1-x}FeO_{3-\delta}$ ($0.71 \leq x < 0.91$) were synthesized. ► $Sr_{0.75}Y_{0.25}Fe_{1-y}M_yO_{3-\delta}$, *M*=Cr, Mn, Ni were prepared. ► High-temperature conductivity properties and crystal structure were studied. ► High-temperature thermal expansion behavior was investigated.

Structural characterization of the perovskite series $Sr_{1-x}La_xTi_{0.5}Mn_{0.5}O_3$

Original Research Article
Pages 39-42
Ilyas Qasim, Brendan J. Kennedy

Graphical abstract

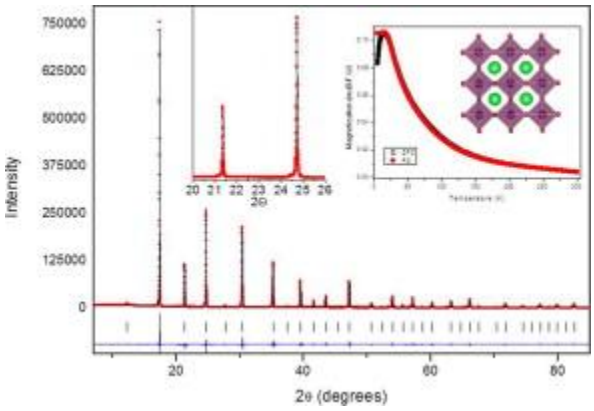

Highlights

► Structural studies of $Sr_{1-x}La_xTi_{0.5}Nb_{0.5}O_3$ perovskites, show lack of long range Mn:Ti order. ► Magnetic properties indicative of spin-glass behavior. ► Changes of crystal structure from cubic to rhombohedral with increasing lanthanum content.

Synthesis, crystal structure and catalytic effect on thermal decomposition of RDX and AP: An energetic coordination polymer $[Pb_2(C_5H_3N_5O_5)_2(NMP)\cdot NMP]_n$

Original Research Article
Pages 43-48
Jin-jian Liu, Zu-Liang Liu, Jian Cheng, Dong Fang

Graphical abstract

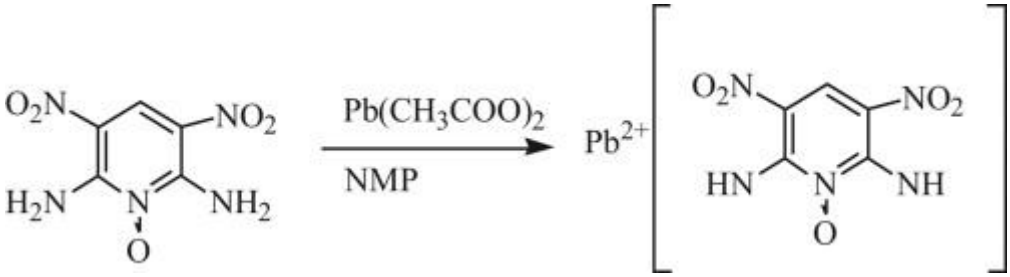

Highlights

► We have synthesized and characterized an energetic lead(II) coordination polymer. ► We have measured its molecular structure and thermal decomposition. ► It has significant catalytic effect on thermal decomposition of AP.

Magnetic behavior of the $Bi_{2-y}Sr_yIr_2O_7$ pyrochlore solid solution

Original Research Article
Pages 49-53
C. Cosio-Castaneda, P. de la Mora, F. Morales, R. Escudero, G. Tavizon

Graphical abstract

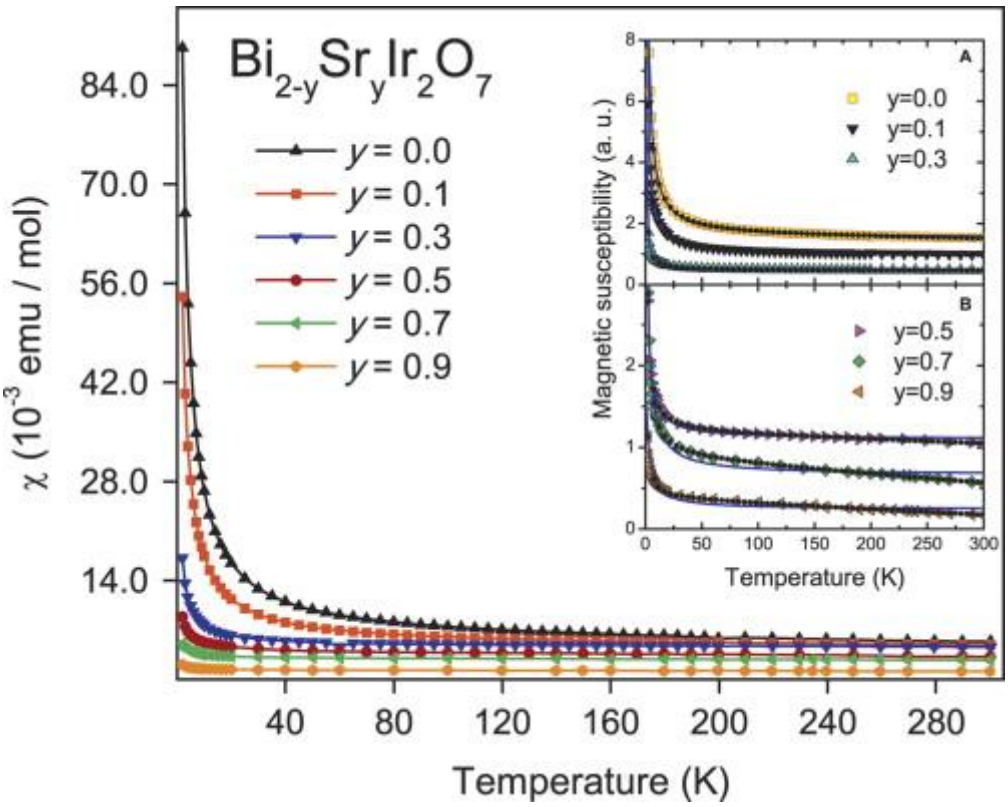

Highlights

► The magnetic susceptibility of the $Bi_{2-x}Sr_xIr_2O_7$ system is discussed. ► No magnetic transition is observed. ► Magnetic measurements on the $Bi_{2-y}Sr_yIr_2O_7$ indicate the existence of Ir^{5+}. ► The magnetic susceptibility does not follow a Curie–Weiss law. ► A modified Curie–Weiss equation describes correctly the magnetic susceptibility.

Color-control of the persistent luminescence of cadmium silicate doped with transition metals

Original Research Article
Pages 54-59
Carolina M. Abreu, Ronaldo S. Silva, Mário E.G. Valerio, Zélia S. Macedo

Graphical abstract

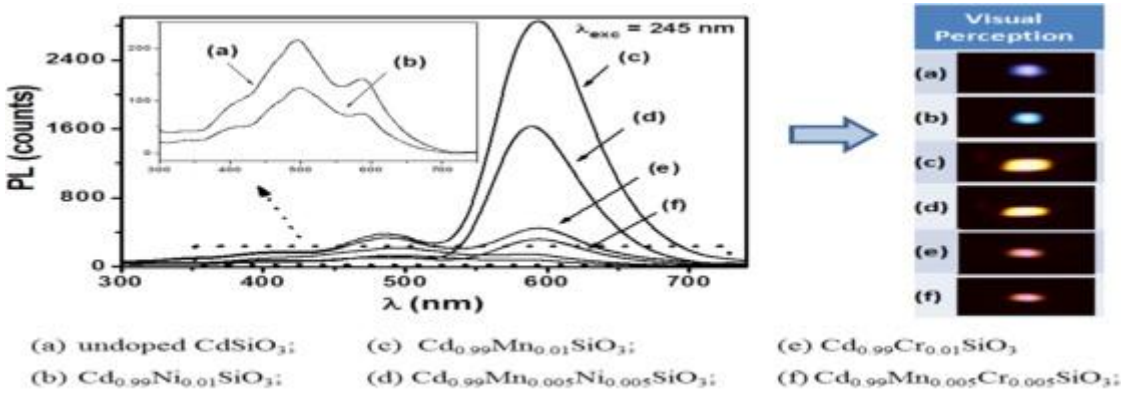

(a) undoped $CdSiO_3$; (c) $Cd_{0.99}Mn_{0.01}SiO_3$; (e) $Cd_{0.99}Cr_{0.01}SiO_3$
(b) $Cd_{0.99}Ni_{0.01}SiO_3$; (d) $Cd_{0.99}Mn_{0.005}Ni_{0.005}SiO_3$; (f) $Cd_{0.99}Mn_{0.005}Cr_{0.005}SiO_3$;

Highlights

► $CdSiO_3$ was doped with Mn, Ni and Cr to produce multicolored phosphors. ► Valence of the dopants was determined as 3+ for Cr, 2+ for Ni and 2+ and 3+ for Mn. ► The presence of absorption bands in the visible region led to self-absorption. ► Self-absorption in some cases can decrease the light output. ► Luminescent channels were created and related to internal transitions of the dopants.

Crystal structure and catalytic properties of three inorganic–organic hybrid constructed from heteropolymolybdate and aminopyridine

Original Research Article
Pages 60-69
Qian Deng, Yilan Huang, Zhenshan Peng, Zengjin Dai, Minru Lin, Tiejun Cai

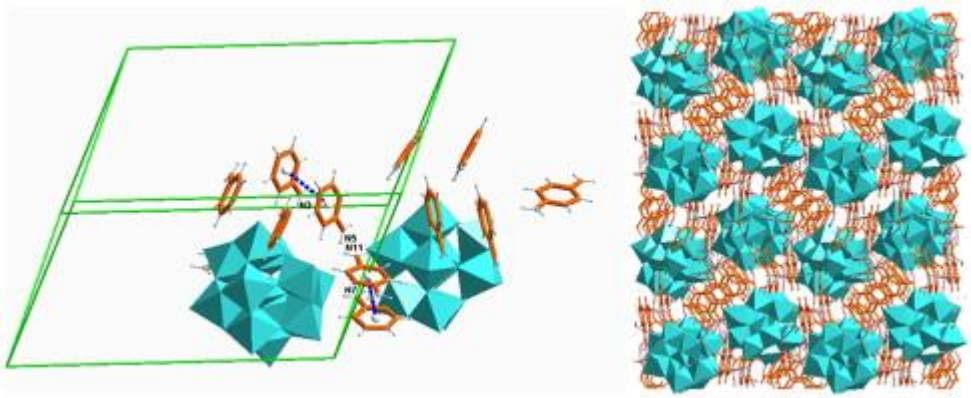

Highlights

► Three 3-D Keggin inorganic–organic hybrid frameworks were synthesized. ► The π–π stacking interactions are existed in Compounds 1 and 2. ► Compound 2 contains a

tetramolecular water cluster connected by hydrogen bond. ► Compounds 1 and 3 are active in the catalytic oxidation of methanol into CO_2 and H_2O.

Insight into cation disorder of $Li_2Fe_{0.5}Mn_{0.5}SiO_4$

Original Research Article
Pages 70-75
Marcella Bini, Stefania Ferrari, Doretta Capsoni, Clelia Spreafico, Cristina Tealdi, Piercarlo Mustarelli

Graphical abstract

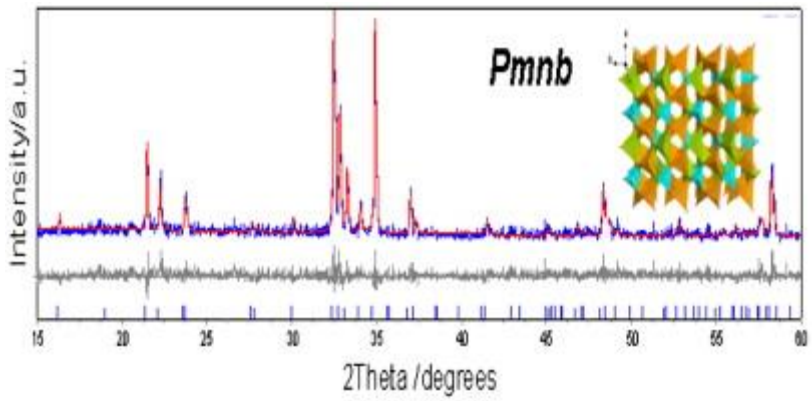

Highlights

► Study of the thermal behavior of $Li_2Fe_{0.5}Mn_{0.5}SiO_4$. ► The anti-site defect does justify the diffraction patterns changes with temperature. ► The *Pmnb* polymorph is stable in the investigated temperaturerange.

Structural, morphological and spectroscopic properties of Eu^{3+}-doped rare earth fluorides synthesized by the hydrothermalmethod

Original Research Article
Pages 76-83
Tomasz Grzyb, Marcin Runowski, Agata Szczeszak, Stefan Lis

Graphical abstract

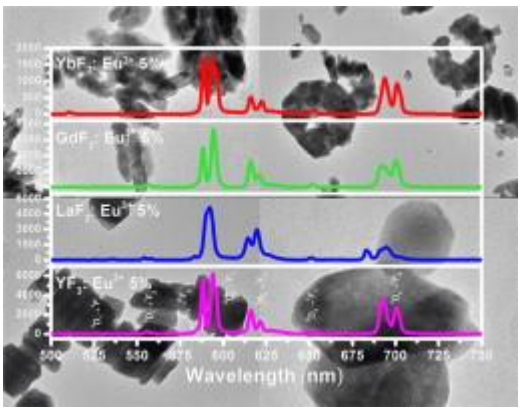

Highlights

► Nanocrystalline fluorides were synthesized using modified hydrothermal method. ► Structural and morphological properties of *in situ* prepared nanomaterials were studied. ► Luminescence properties of $RE F_3:Eu^{3+}$ (*RE*=Y, La, Gd, Yb) were compared and investigated.

Investigations on the growth and characterization of vertically aligned zinc oxide nanowires by radio frequency magnetronsputtering

Original Research Article
Pages 84-89
P. Sundara Venkatesh, K. Jeganathan

Graphical abstract

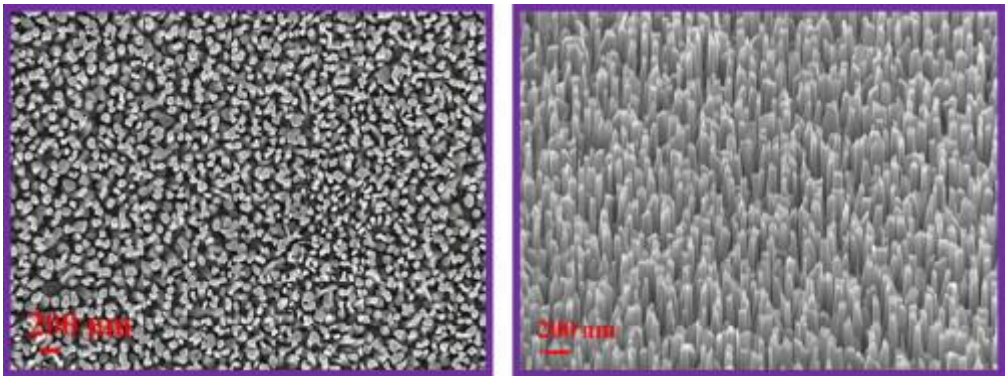

Highlights

► ZnO nanowires have been grown by rf magnetron sputtering. ► A morphologically superior and coalescence free ZnO nanowires have been realized. ► ZnO nanowires exhibit hexagonal wurtzite crystal structure. ► A dominant visible emission indicates the presence of point defects in nanowires.

Synthesis and characterization of thermally stable large-pore mesoporous nanocrystallineanatase

Original Research Article
Pages 90-98
Natalia I. Ermokhina, Vitaly A. Nevinskiy, Piotr A. Manorik, Vladimir G. Ilyin, Viktor N. Novichenko, Mykola M. Shcherbatiuk, Dmitro O. Klymchuk, Mykola M. Tsyba, Alexander M. Puziy

Graphical abstract

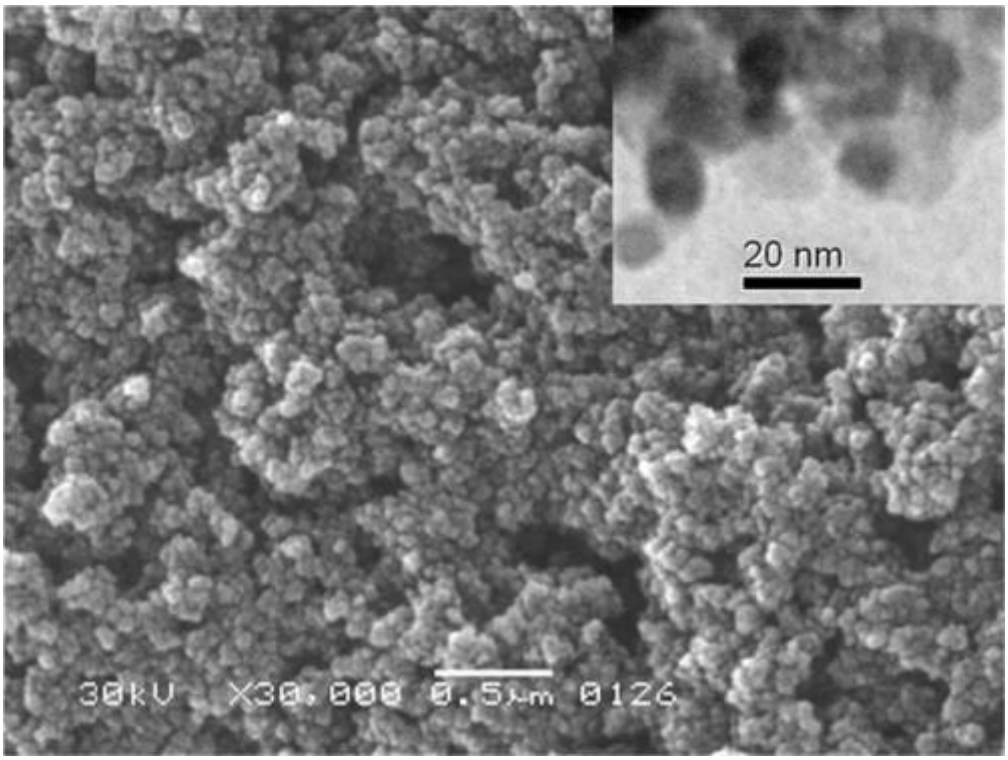

Highlights

► Large-pore mesoporous nanocrystalline TiO_2 was obtained by sol–gel synthesis. ► Crown ether was used as template in presence of surfactant and/or La^{3+} ions. ► Anatase (crystalline size<11 nm) is the only crystalline phase present in TiO_2. ► TiO_2 shows well-defined homogeneous spherical morphology (micro- and nano-spheres).

Supramolecular assembly of borate with quaternary ammonium: Crystal structure and tunable luminescent properties

Original Research Article
Pages 99-104
Jie Liang, Yong-gang Wang, Ying-xia Wang, Fu-hui Liao, Jian-hua Lin

Graphical abstract

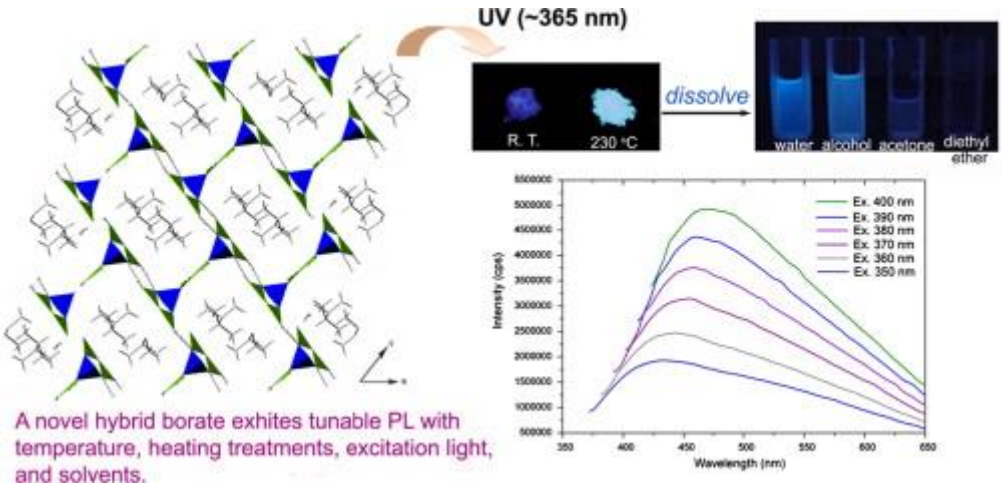

Highlights

► A novel quaternary ammonium borate was synthesized. ► It possesses a supramolecular network fomed by H-bonded $[B_5O_6(OH)_4]^-$ anions. ► This borate shows tunable luminescent properties with temperature, heating treatment, excitation light, and solvents.

The dimeric $[V_2O_2F_8]^{4-}$ anion: Structural characterization of a magnetic basic-building-unit

Original Research Article
Pages 105-109
Hongcheng Lu, Romain Gautier, Zuo-Xi Li, Wanqi Jie, Zhengtang Liu, Kenneth R. Poeppelmeier

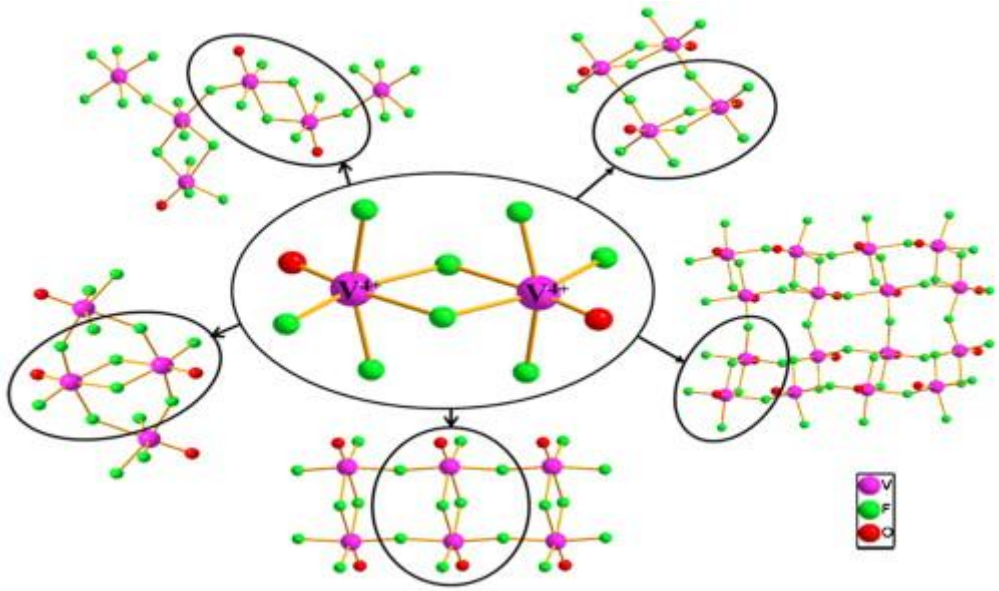

Highlights

► A new vanadium oxyfluoride was synthesized by hydrothermal method. ► The Dimeric $[V_2O_2F_8]^{4-}$ basic building unit is isolated in the hydrogen bond networks. ► The coordination of $[V_2O_2F_8]^{4-}$ units to the extended structure is investigated. ► Isolated $[V_2O_2F_8]^{4-}$ units exhibit antiferromagnetic coupling.

Structural and magnetic properties of the $M_2Ga_2Fe_2O_9$ (M=In, Sc) oxides

Original Research Article
Pages 110-116
Monica Ciomaga Hatnean, Loreynne Pinsard-Gaudart, Maria Theresa Fernández-Díaz, Sylvain Petit, Ambesh Dixit, Gavin Lawes, R. Suryanarayanan

Graphical abstract

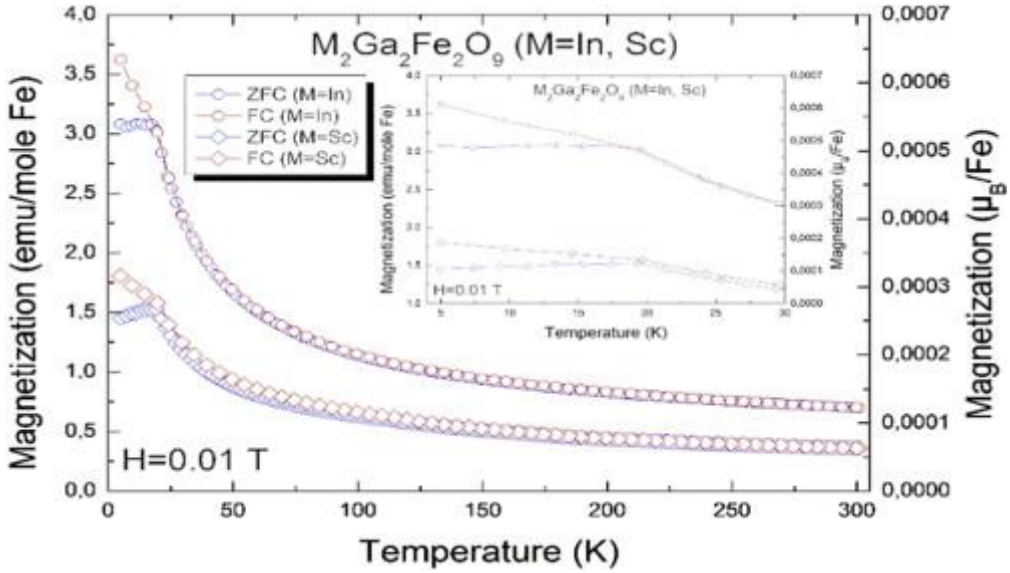

Highlights

► Chemical disorder study of the $M_2Ga_2Fe_2O_9$ (M=In, Sc) compounds. ► Our study indicates for the first time a glassy magnetic ground state of this system. ► The glassy-like-behavior is due to magnetic frustration created by the site disorder.

Surface decoration through electrostatic interaction leading to enhanced reactivity: Low temperature synthesis of nanostructured chromium borides (CrB and CrB_2)

Original Research Article
Pages 117-122

Menaka, Bharat Kumar, Sandeep Kumar, A.K. Ganguli

Graphical abstract

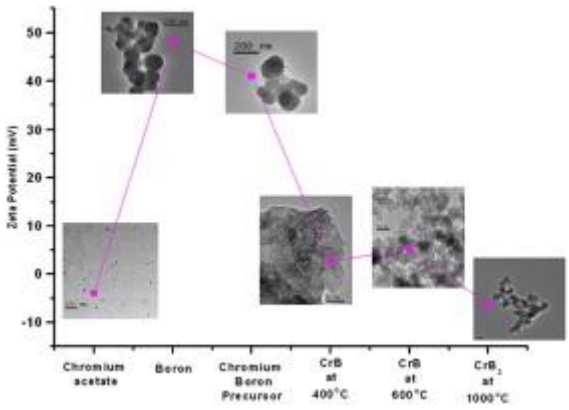

Highlights

► Novel borothermal reduction process for synthesis of chromium boride. ► Significant lowering of reaction temperature to obtain nanocrystalline chromium boride. ► Enhanced reactivity due to appropriate surface interactions.

Controlled synthesis and formation mechanism of monodispersive lanthanum vanadate nanowires with monoclinic structure

Original Research Article
Pages 123-127
Li Tian, Qiliang Sun, Xijun Xu, Yaolin Li, Yunfei Long, Guangshan Zhu

Graphical abstract

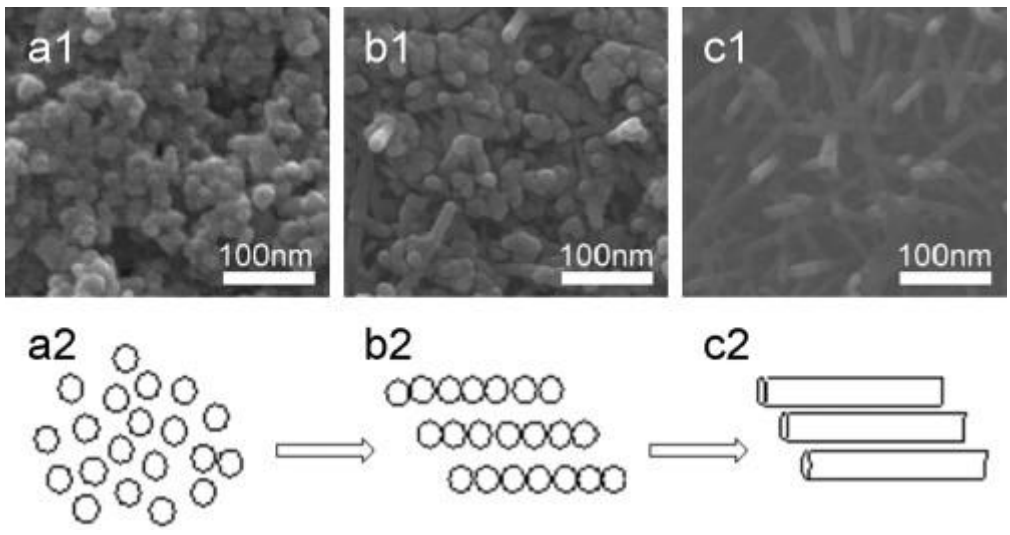

Highlights

► Monodisperse $LaVO_4$ nanowires with high aspect ratio have been prepared solvothermally without any templates. ► The morphology and structure of $LaVO_4$ nanowires were characterized by XRD, SEM, TEM techniques. ► The formation mechanism of $LaVO_4$ nanowires is suggested that oriented attachment plays a vital role.

Effect of Cu^{2+} and Ni^{2+} substitution at the Mn site in $(La_{0.63}Ca_{0.37})MnO_3$: A neutron powder diffraction investigation

Original Research Article
Pages 128-135
A. Martinelli, M. Ferretti, C. Castellano, M.R. Cimberle, C. Ritter

Graphical abstract

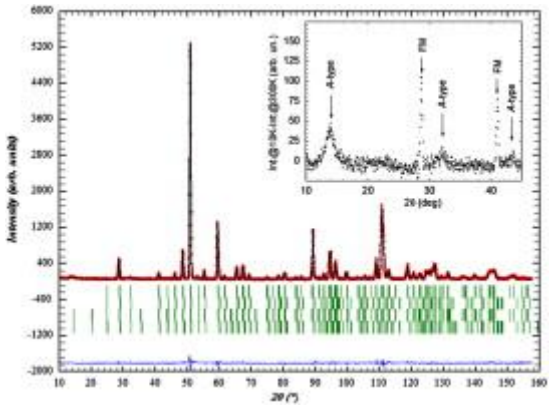

Highlights

► $(La_{0.63}Ca_{0.37})MnO_3$ was substituted with Ni and Cu. ► Neutron powder diffraction and Rietveld refinement were carried out. ► A quantum critical point possibly occurs in the $(La_{0.63}Ca_{0.37})(Mn_{1-x}Cu_x)O_3$ system.

Self-assembled flower-like antimony trioxide microstructures with high infrared reflectance performance

Original Research Article
Pages 136-142
Shengsong Ge, Xiaokun Yang, Qian Shao, Qingyun Liu, Tiejun Wang, Lingyun Wang, Xiaojie Wang

Graphical abstract

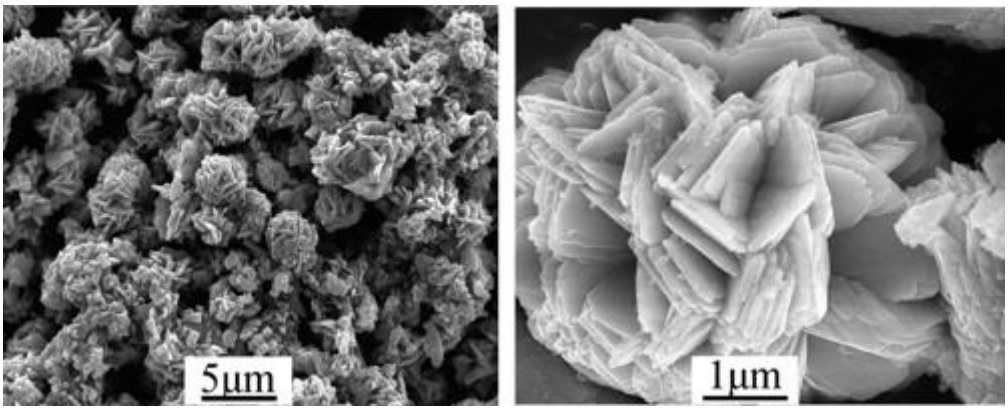

Highlights

► Uniform flower-like microstructures were synthesized via simple hydrothermal reaction. ► The flower-like Sb_2O_3 microstructures exhibited higher reflectivity than other morphologies under the UV–vis–NIR light. ► Influencing parameters on the Sb_2O_3 morphologies have been discussed in detail. ► Possible mechanism leading to flower-like microstructures was proposed.

($Na_xk_{1-x})_2Ta_4O_{11}$ ($x \approx 0.93$) piezoelectric phase from the transformation of Ta_2O_5 thin films of monoclinic structure

Original Research Article
Pages 143-149
M. Le Gallic, H. Roussel

Graphical abstract

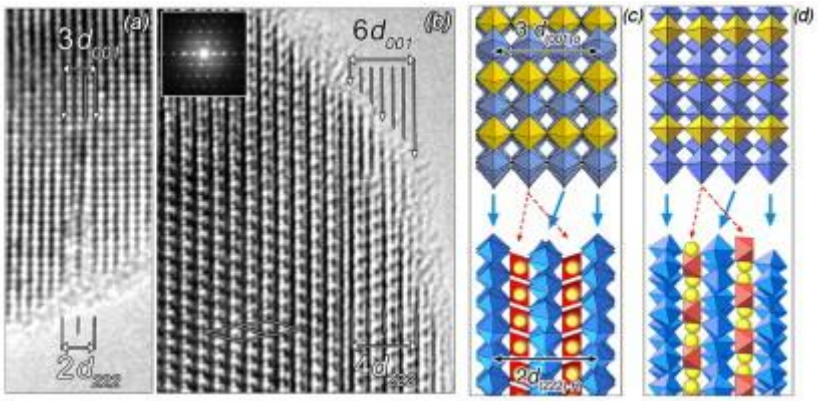

Highlights

► The formation of a piezoelectric phase in Ta_2O_5 thin films, reported in previous articles, is re-examined. ► Its composition is actually ($Na_x,K_{1-x})_2Ta_4O_{11}$ with x=0.93, instead of Ta_2O_5. ► Ta^{5+} vacancies, compensated by protons within tantalumoxide, are involved in a new analysis of the transformation.

Vapour phase approach for iron oxide nanoparticle synthesis from solid precursors

Original Research Article
Pages 150-156
Mandeep Singh, Pavel Ulbrich, Vadym Prokopec, Pavel Svoboda, Eva Šantavá, František Štěpánek

Graphical Abstract

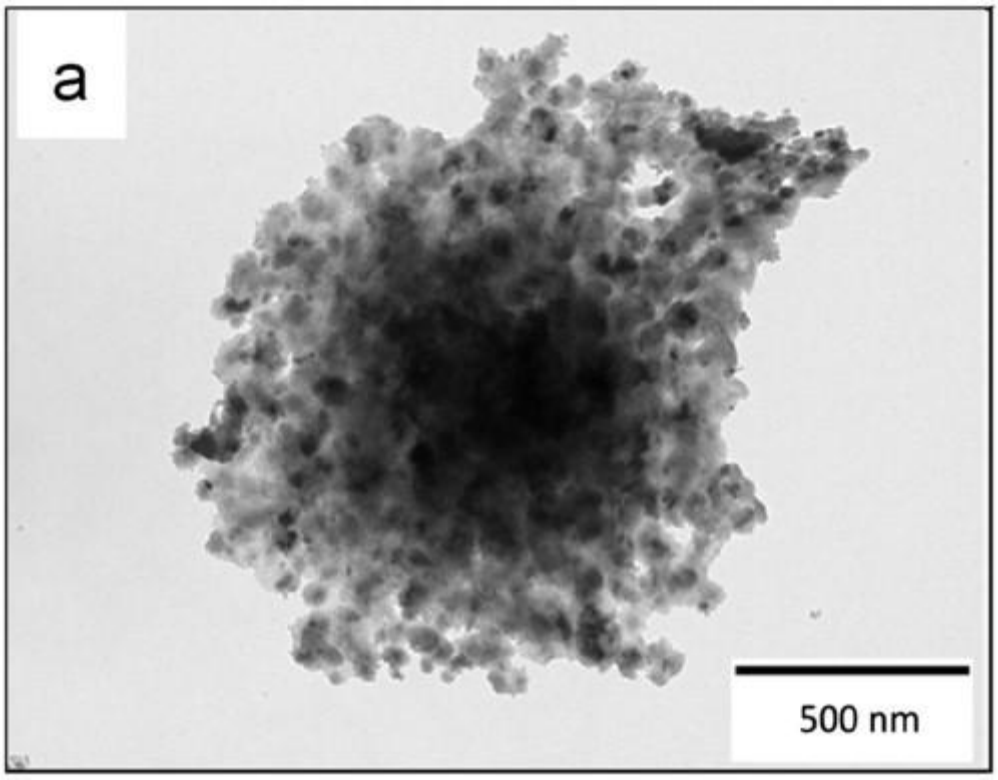

Highlights

► Novel vapour phase (non-solvent) approach for iron oxide nanoparticle synthesis. ► Attractive alternative approach to the present co-precipitation method. ► Better magnetic properties with high coercivity of nanoparticles. ► A high specific absorption rate (SAR) for hyperthermia applications.

Crystal structure and phase transition mechanisms in $CsFe_2F_6$

Original Research Article
Pages 157-164
M.S. Molokeev, E.V. Bogdanov, S.V. Misyul, A. Tressaud, I.N. Flerov

Graphical abstract

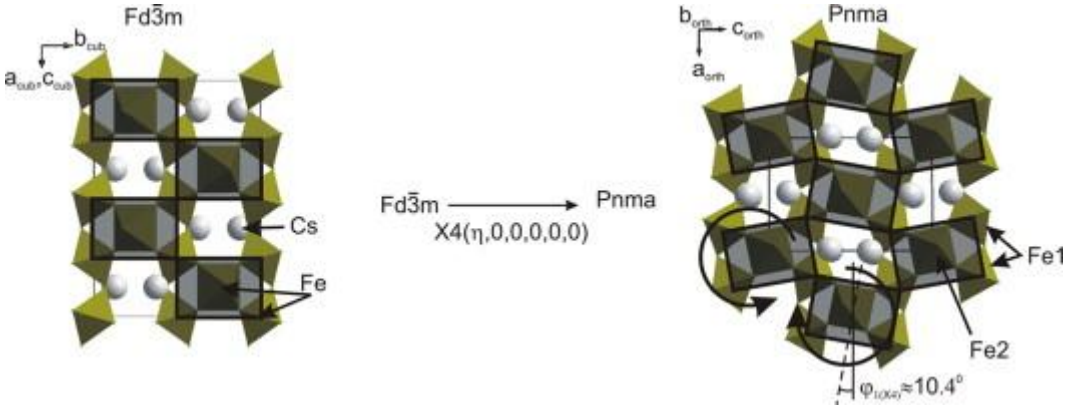

Highlights

► Structural transition found for the first time in $CsFe_2F_6$ with defect pyrochlore type. ► Fe^{II} and Fe^{III} atoms are ordered in room temperature *Pnma* form of $CsFe_2F_6$. ► *Pnma*(*Z*=4)→*Imma*(*Z*=4)→$I4_1$/*amd*(*Z*=4)→*Fd*-3*m*(*Z*=8) transition sequence is proposed. ► Structural transition due to rotation of MF_6 groups+small displacements of Fe atoms. ► The low value of the entropy is in agreement with a displacive-type transition.

Improved synthesis and characterization of the copper Lyonsite-type compound $Cu_{4-x}Mo_3O_{12}$

Original Research Article
Pages 165-169
Adam D. Raw, James A. Ibers, Kenneth R. Poeppelmeier

Graphical abstract

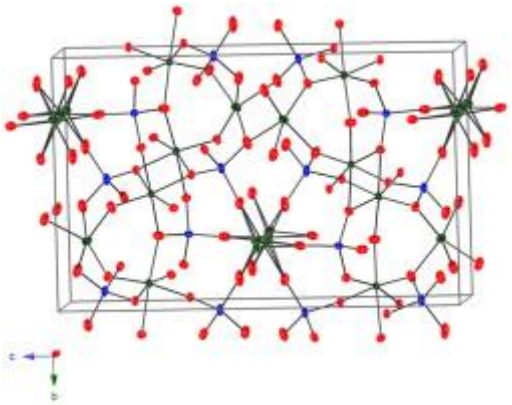

Highlights

► A repeatable method for the synthesis $Cu_{3.82(1)}Mo_3O_{12}$ has been developed. ► Single crystals were formed from a polycrystalline sample through the use of a gallium flux. ► Thermopower measurements of $Cu_{3.82(1)}Mo_3O_{12}$ show n-type behavior.

On the densification of cubic ZrO_2 nanocondensates by capillarity force and turbostratic C–Si–H multiple shell

Original Research Article
Pages 170-178
Chao-Hsien Wu, Shuei-Yuan Chen, Pouyan Shen

Graphical abstract

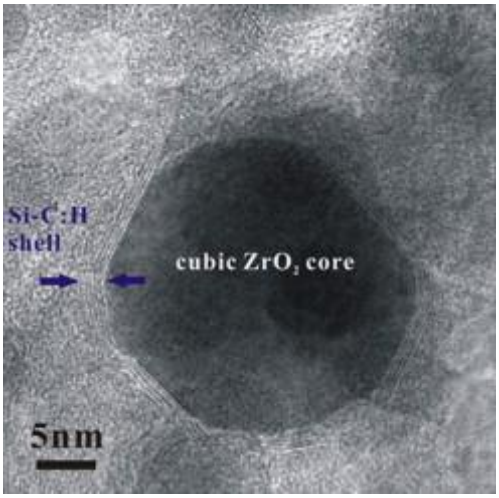

Highlights

► Turbostratic C–Si–H lamellar phase and ZrO_2 condensates were synthesized by PLA. ► The c-ZrO_2 phase ca. 10% denser than the ambient lattice was stabilized as 3–10 nm. ► The c-ZrO_2 particles up to 30 nm were densified when encapsulated by the $C_{1-x}Si_x$:H multiple shell. ► Tight ion binding of the c-ZrO_2 due to capillarity force and turbostratic shell.

Facile synthesis of hollow zeolite microspheres through dissolution–recrystallization procedure in the presence of organosilanes

Original Research Article
Pages 179-188
Haixiang Tao, Jiawen Ren, Xiaohui Liu, Yanqin Wang, Guanzhong Lu

Graphical abstract

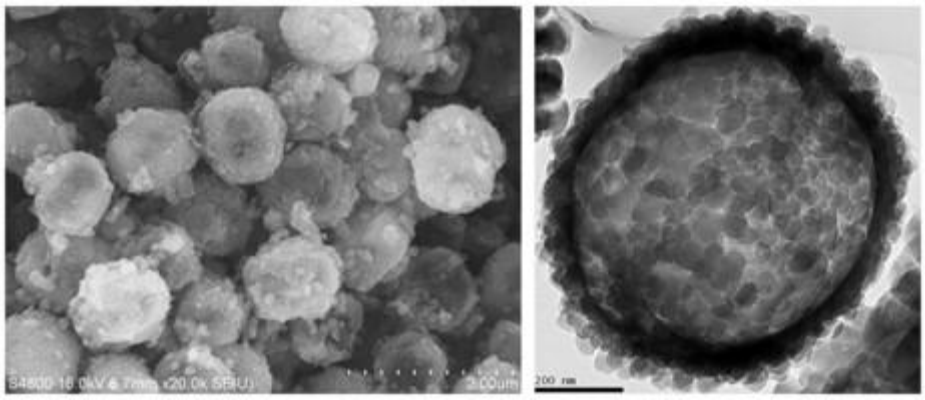

Highlights

► Hollow zeolite spheres with aggregated zeolite nanocrystals were synthesized via a dissolution–recrystallization procedure. ► Organosilane influences both the morphology and hollow structure of zeolite spheres. ► Hollow zeolite spheres showed an excellent catalytic performance in alkylation of toluene with benzyl chloride.

A comparison of the photocatalytic activity of six tunneled titanates

Original Research Article
Pages 189-196
Stephen Sanford, Scott T. Misture, Doreen D. Edwards

Graphical abstract

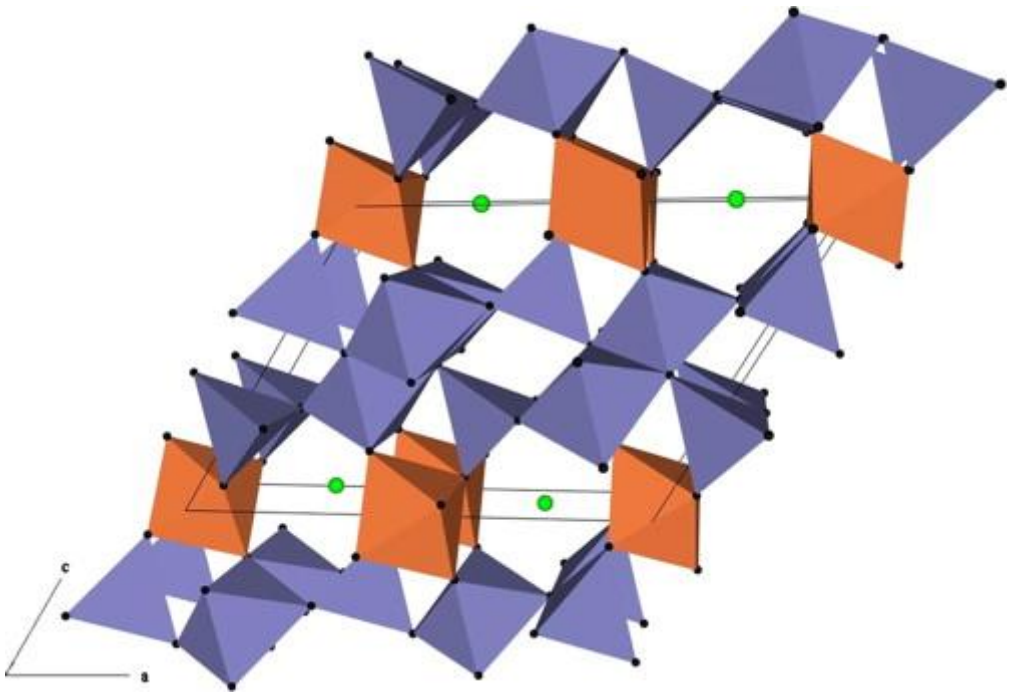

Highlights

► The photocatalytic activity of six tunneled titanates was compared. ► $Na_{0.8}Ga_{4.8}Ti_{1.2}O_{10}$ and $Na_{0.7}Ga_{4.7}Ti_{0.3}O_8$ exhibited negligible photocatalytic activity. ► The activities of $Na_{0.8}Ga_{4.8}Ti_{2.2}O_{12}$, $KGa_{17}Ti_{15}O_{56}$, and $K_{1.5}Ga_{1.5}Ti_{6.5}O_{16}$ were similar to each other. ► $BaTi_4O_9$ exhibited the highest photocatalytic activity. ► Photocatalytic activity is related to the density of TiO_6 octahedra.

A novel polythreading Ag(I) coordination polymer with blue photoluminescence

Original Research Article
Pages 197-201
Xian-Ying Duan, Jing Yao, Chang-Sheng Lu, Qing-Jin Meng

Graphical abstract

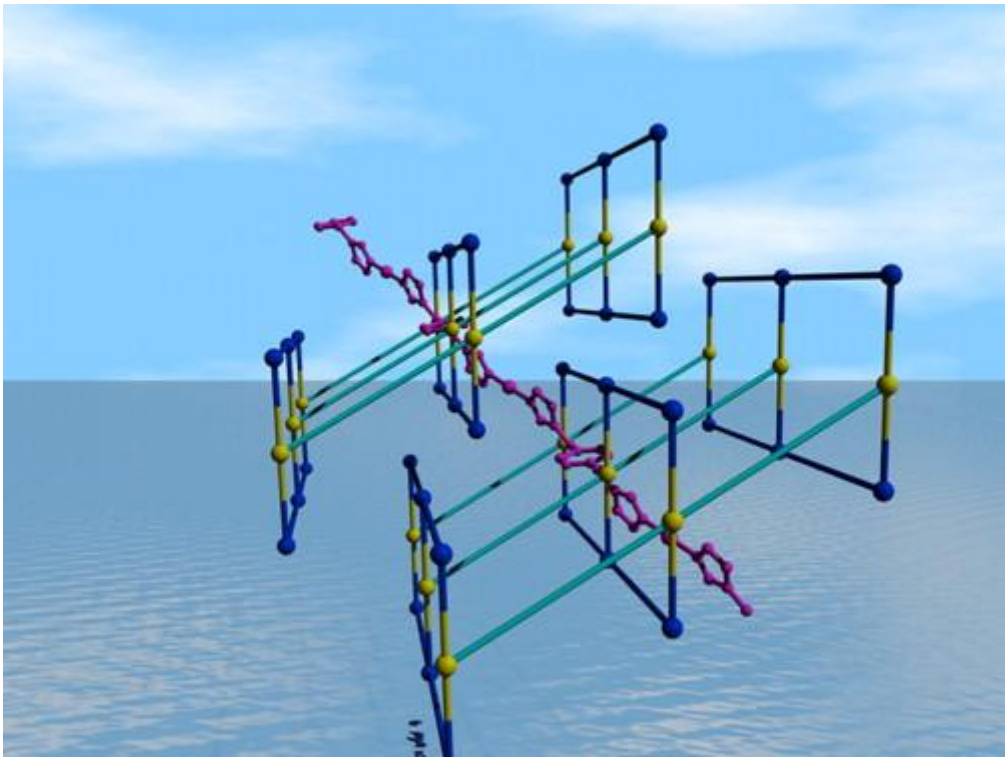

Highlights

► Novel $1D^{+}+2D^{-}\rightarrow 3D$ polythreading coordination complex was reported. ► Diverse conformations of *p*-bix result in different 1D $[Ag(p\text{-bix})]_{\infty}^{+}$ chains. ► The title complex displayed blue photoluminescence at room temperature.

Structural differences existing in bulk and nanoparticles of $Y_2Sn_2O_7$: Investigated by experimental and theoretical methods

Original Research Article
Pages 202-208
Sandeep Nigam, V. Sudarsan, C. Majumder, R.K. Vatsa

Graphical abstract

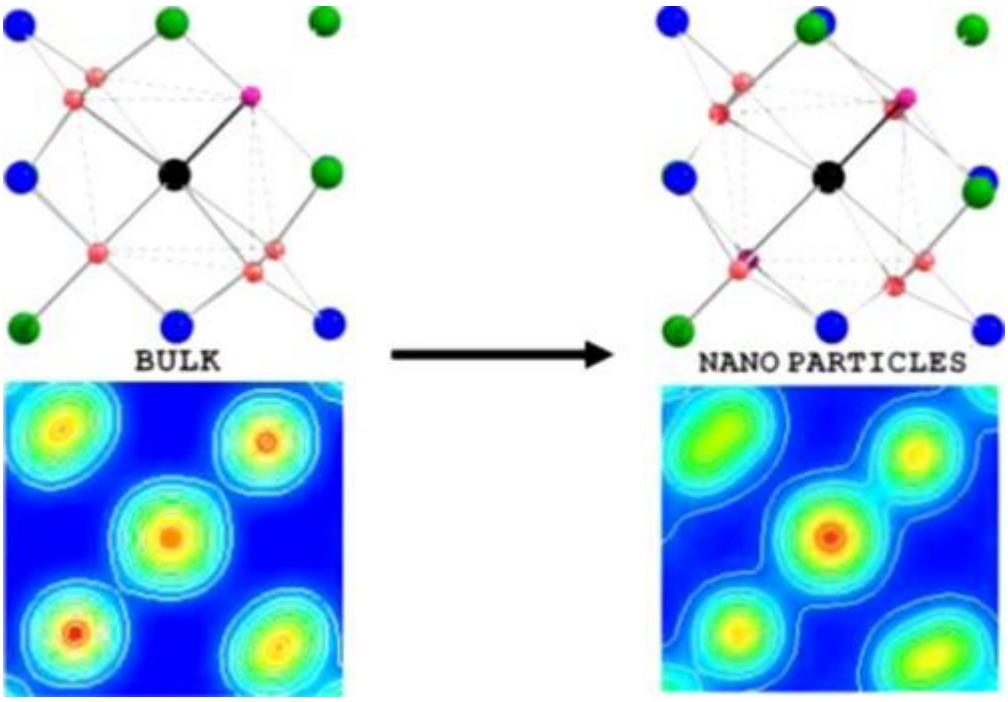

Highlights

► YO_8 scalenohedron is axially and equatorially distorted in $Y_2Sn_2O_7$ nanoparticles. ► Enlargement of SnO_6 octahedron in nanoparticles of $Y_2Sn_2O_7$ compared to bulk. ► Less symmetric charge distribution around Y^{3+} ions in $Y_2Sn_2O_7$ nanoparticles.

Drastic changes in electronic, magnetic, mechanical and bonding properties from Zr_2CoH_5 to Mg_2CoH_5

Original Research Article
Pages 209-214
Samir F. Matar

Graphical Abstract

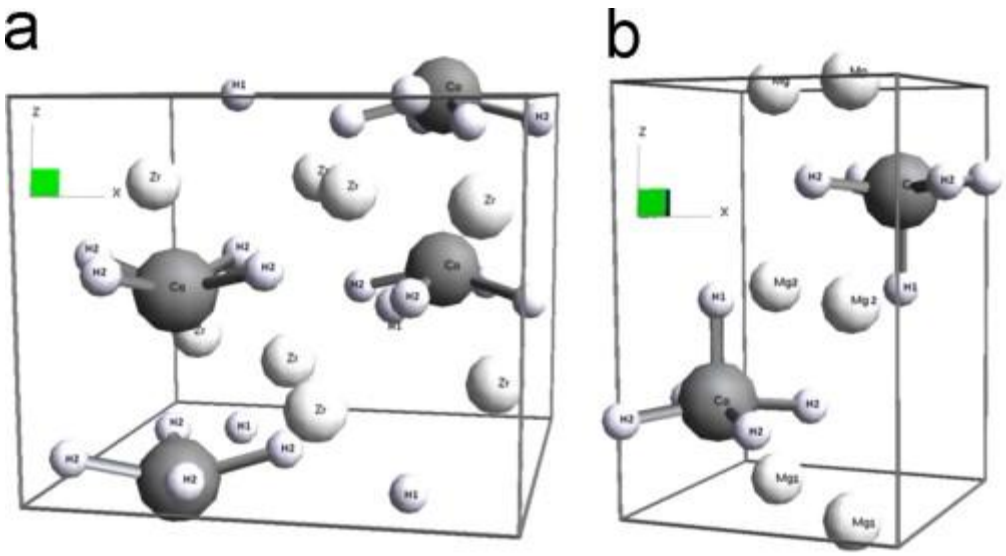

Highlights

► Zr_2CoH_5 and Mg_2CoH_5 show contrasted electronic, magnetic, mechanical and bonding properties. ► Zr_2CoH_5 is found more cohesive, harder and less ductile than Mg_2CoH_5. ► Metallic ferromagnet Zr_2CoH_5 in contrast with non-magnetic and insulating Mg_2CoH_5.

A neutron diffraction study of structural distortion and magnetic ordering in the cation-ordered perovskites $Ba_2Nd_{1-x}Y_xMoO_6$

Original Research Article
Pages 215-220
Oonagh M. Collins, Edmund J. Cussen

Graphical Abstract

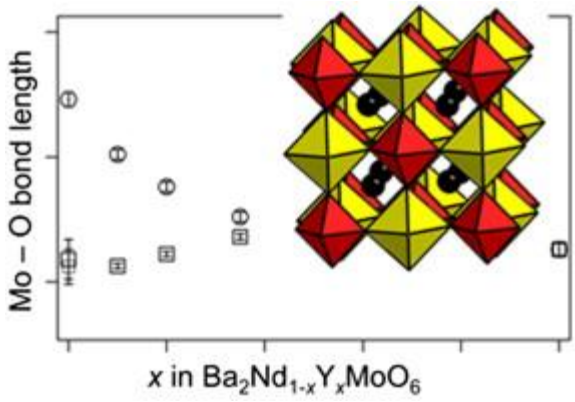

Highlights

► Introducing Y^{3+} into Ba_2NdMoO_6 stabilises tetragonal symmetry to 2 K. ► A distortion of the ligand field around the Mo^{5+} $4d^1$ cation confers electronic stabilisation. ► The size of the distortion is progressively reduced with increasing Y^{3+} content. ► Distortion gives negative thermal expansion along *z* and antiferromagnetic order at $T \leq 15$ K.

Structure and optical properties of cubic gallium oxynitride synthesized by solvothermal route

Original Research Article
Pages 221-226
Andreas Oberländer, Isabel Kinski, Wenliang Zhu, Giuseppe Pezzotti, Alexander Michaelis

Graphical abstract

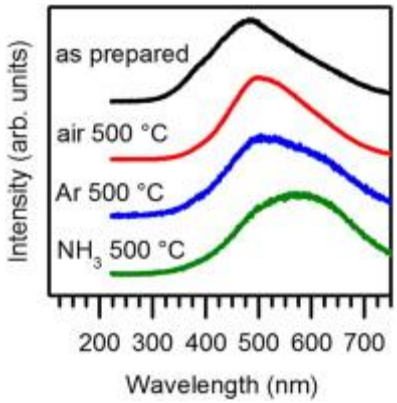

Highlights

► Raman spectrum of cubic gallium oxynitride. ► Experimental determination of optical band gap. ► Shift of band gap energy due to heat treatment. ► Nitrogen incorporation leads to deep level acceptor states. ► Red shifted luminescence spectrum.

Structural properties of mixed $(NH_4)_{2-x}Rb_xZnCl_4$ (x=0, 1, and 2) crystals studied by ^1H and ^{87}Rb nuclear magnetic resonance

Original Research Article
Pages 227-231
Ae Ran Lim, Kye-Young Lim

Graphical abstract

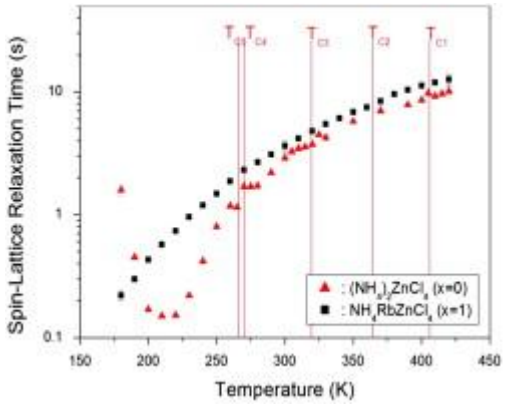

Highlights

► Mixed $(NH_4)_{2-x}Rb_xZnCl_4$ (x=0, 1, and 2) crystals. ► The crystallographic structures by occupation probabilities. ► The NH_4 and Rb occupation rates.

Silver vanadium diphosphate $Ag_2VP_2O_8$: Electrochemistry and characterization of reduced material providing mechanistic insights

Original Research Article
Pages 232-240
Esther S. Takeuchi, Chia-Ying Lee, Po-Jen Cheng, Melissa C. Menard, Amy C. Marschilok, Kenneth J. Takeuchi

Graphical abstract

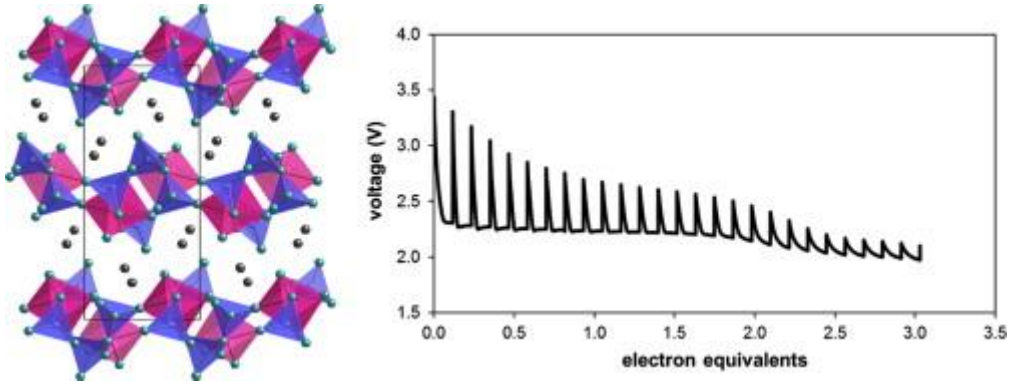

Highlights

► First electrochemical study of a silver vanadium diphosphate, $Ag_2VP_2O_8$. ► In-situ formation of Ag^0 nanoparticles was observed upon electrochemical reduction. ► Structural analysis used to provide insight of the electrochemical behavior.

Synchrotron X-ray diffraction study of the $Ba_{1-x}SrSnO_3$ solid solution

Original Research Article
Pages 241-245
Anti K. Prodjosantoso, Qingdi Zhou, Brendan J. Kennedy

Graphical abstract

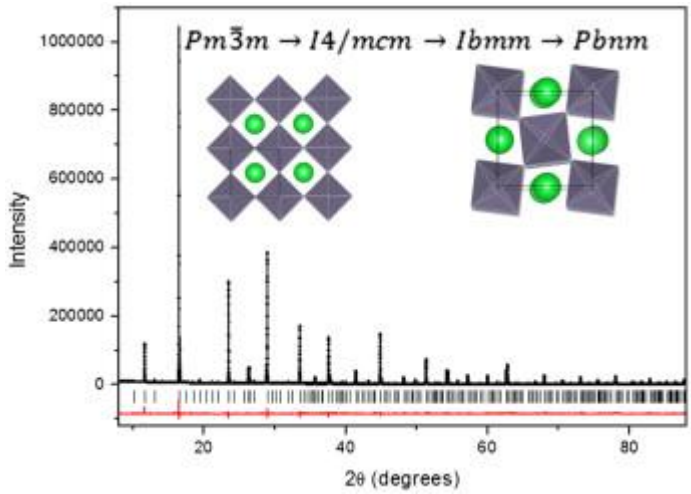

Highlights

► Structures of the stannate perovskites $Ba_{1-x}SrSnO_3$ refined from synchrotron XRD. ► The sequence *Pm*3*m*→*I*4/*mcm*→*Ibmm*→*Pbnm* results from tilting of the octahedra. ► The tilting maintains optimal bonding of the cations seen from the BVS analysis.

The novel phase transition of $NaBi(WO_4)_2$ under high pressure

Original Research Article
Pages 246-250
Chunli Ma, Hang Cui, Fangfei Li, Jingshu Wang, Xiaoxin Wu, Jian Zhang, Qiang Zhou, Jinghe Liu, Qiliang Cui

Graphical abstract

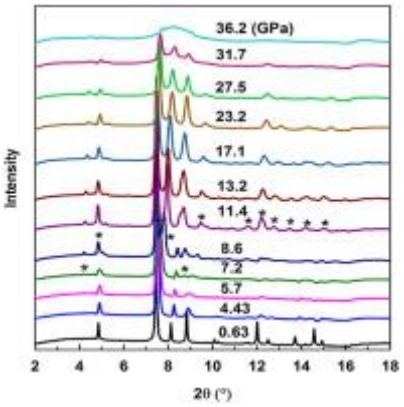

Highlights

► Raman and X-ray diffraction studies performed on $NaBi(WO_4)_2$ up to 30.7 and 36.2 GPa, respectively. ► The tetragonal ($I4_1/a$) into monoclinic ($P2/m$) phase transition is determined. ► With pressure higher than 29 GPa, the $NaBi(WO_4)_2$ ultimately turns into amorphous state. ► The ambient pressure bulk modulus and volume of tetragonal and monoclinic phases are obtained.

Three new Ag(I) coordination architectures based on mixed ligands: Syntheses, structures and photoluminescent properties

Original Research Article
Pages 251-257
Yamin Li, Changyu Xiao, Shu Li, Qi Chen, Beibei Li, Qian Liao, Jingyang Niu

Graphical abstract

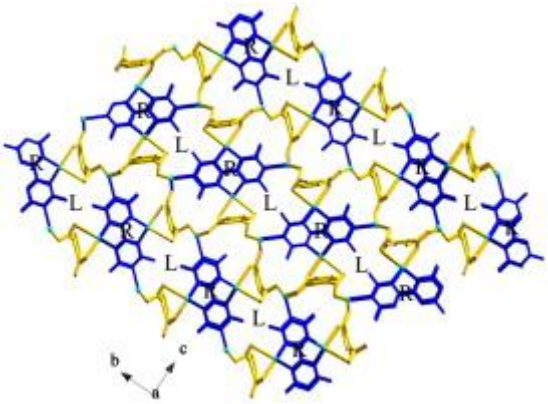

Highlights

► The compound **1** exhibits a novel chiral 3D network with two kinds of single helical chains. ► 3D or 2D new Ag coordination complexes. ► The photoluminescent properties have been measured.

Improve the open-circuit voltage of ZnO solar cells with inserting ZnS layers by two ways

Original Research Article
Pages 258-264
Yunfei Sun, Jinghai Yang, Lili Yang, Jian Cao, Ming Gao, Zhiqiang Zhang, Zhe Wang, Hang Song

Graphical abstract

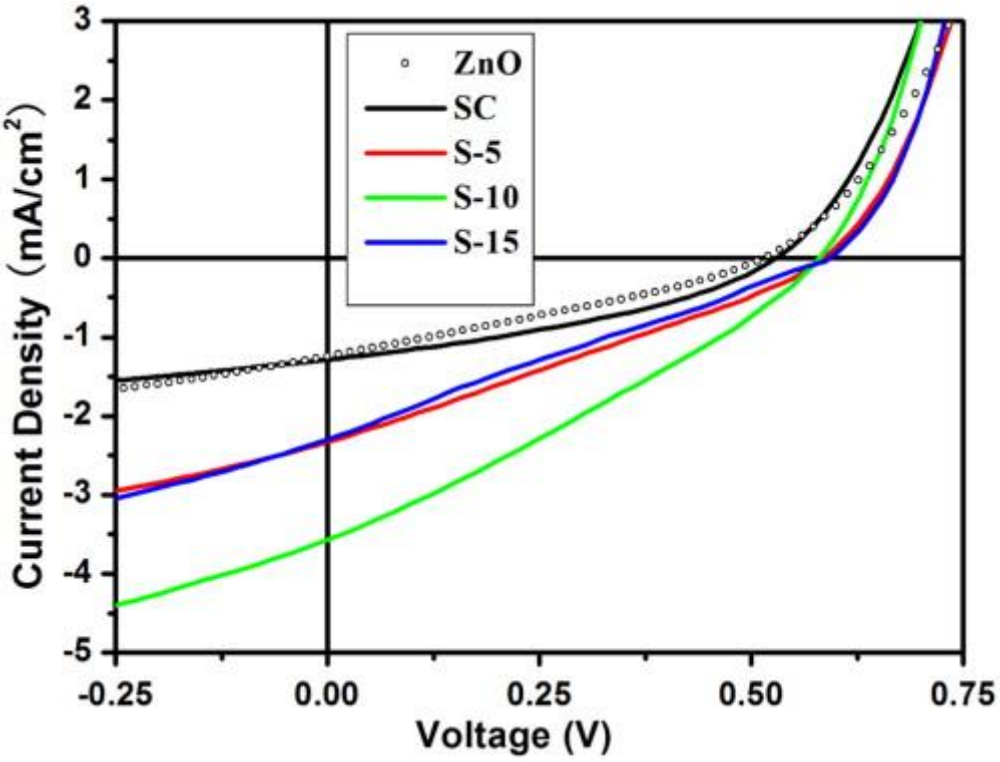

Highlights

► ZnS layers were deposited with two different ways. ► The way of SILAR is more beneficial for retarding the back transfer of electrons. ► The open-circuit voltage increased to 0.59 V by introducing a ZnS layer through SILAR method.

Topological evolution and photoluminescent properties of a series of divalent zinc-based metal–organic frameworks tuned via ancillary ligating spacers

Original Research Article
Pages 265-270
Xiao-Min Lian, Wen Zhao, Xiao-Li Zhao

Graphical abstract

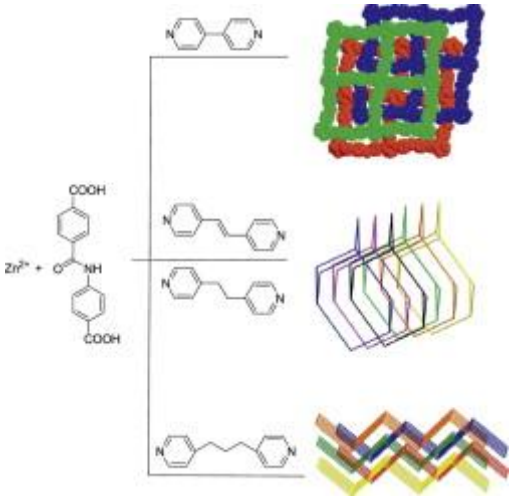

Highlights

► The effect of the pyridyl-based spacers on the formation of MOFs was explored. ► Fine tune over the topology of the MOFs was achieved. ► An interesting structure of 2D→3D parallel polycatenation is reported.

Crystal structure and properties of high-pressure-synthesized $BiRhO_3$, $LuRhO_3$, and $NdRhO_3$

Original Research Article
Pages 271-278
Wei Yi, Qifeng Liang, Yoshitaka Matsushita, Masahiko Tanaka, Xiao Hu, Alexei A. Belik

Graphical abstract

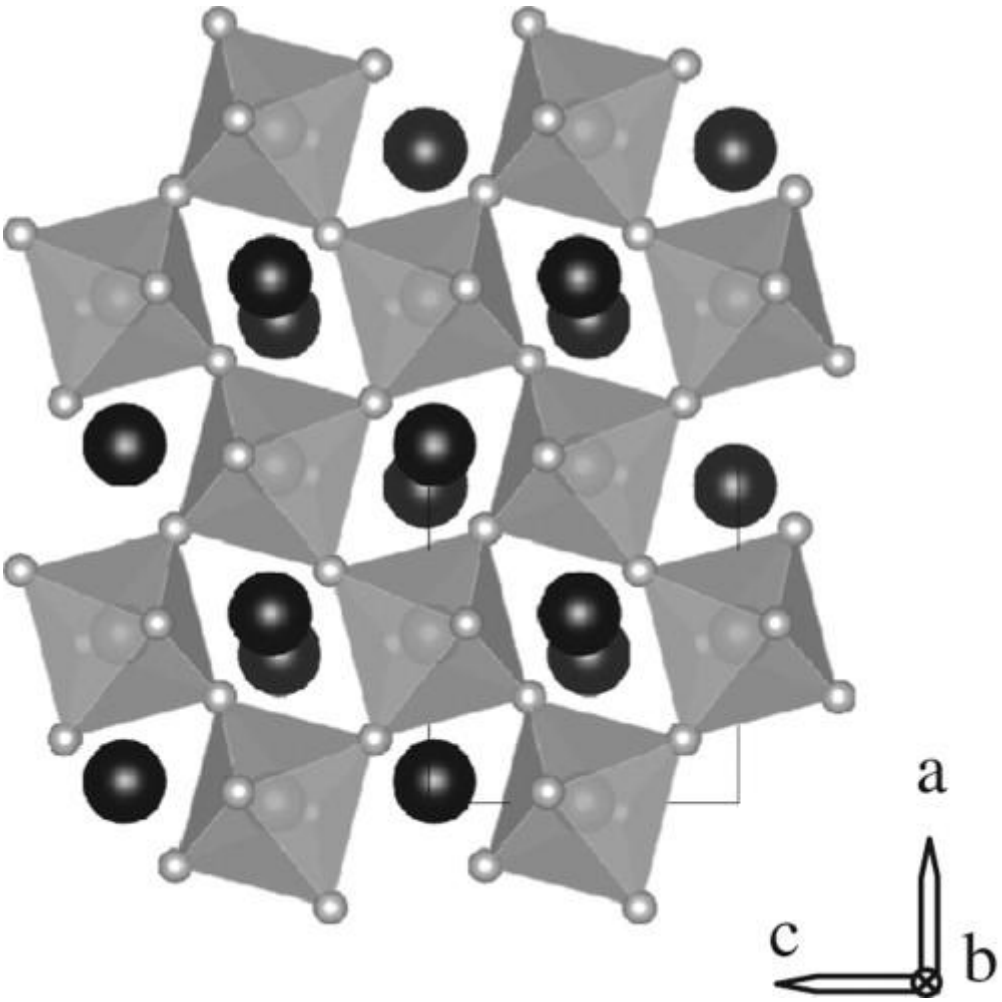

Highlights

► $BiRhO_3$, $LuRhO_3$, and $NdRhO_3$ were prepared using a high-pressure technique. ► Structure of three compounds was determined: centrosymmetric space group *Pnma*. ► $BiRhO_3$ and $LuRhO_3$ are non-magnetic, and $NdRhO_3$ shows paramagnetic behavior. ► Specific heat of $BiRhO_3$, $LuRhO_3$, and $NdRhO_3$ was investigated. ► $BiRhO_3$ has an energy gap of about 1.3 eV.

Effect of *p–d* hybridization, structural distortion and cation electronegativity on electronic properties of $ZnSnX_2$ (*X*=P, As, Sb) chalcopyrite semiconductors

Original Research Article
Pages 279-286
S. Mishra, B. Ganguli

Graphical abstract

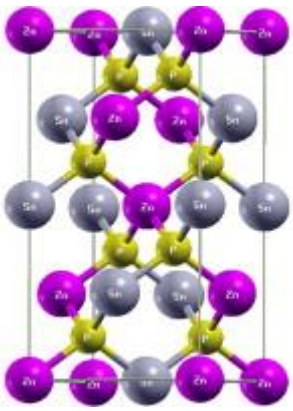

Highlights

► $ZnSnX_2$ (X=P, As, Sb) are direct band gap semiconductors. ► These have band gaps of 1.23 eV, 0.68 eV and 0.19 eV respectively. ► The band gap reduction due to p–d hybridization is 13.41%, 18.51% and 40% respectively. ► Band gap reduction due to structural distortion is 12.12%, 11.11% and 16.66% respectively. ► Band gap increases 8.38%, 3.70% and 21.31% respectively due to cation electronegativity.

90° Rotation of orbital stripes in bilayer manganite $PrCa_2Mn_2O_7$ studied by *in situ* transmission electron microscopy

Original Research Article
Pages 287-293
Z.B. He, G. Deng, H. Tian, Q. Xu, G. Van Tendeloo

Graphical abstract

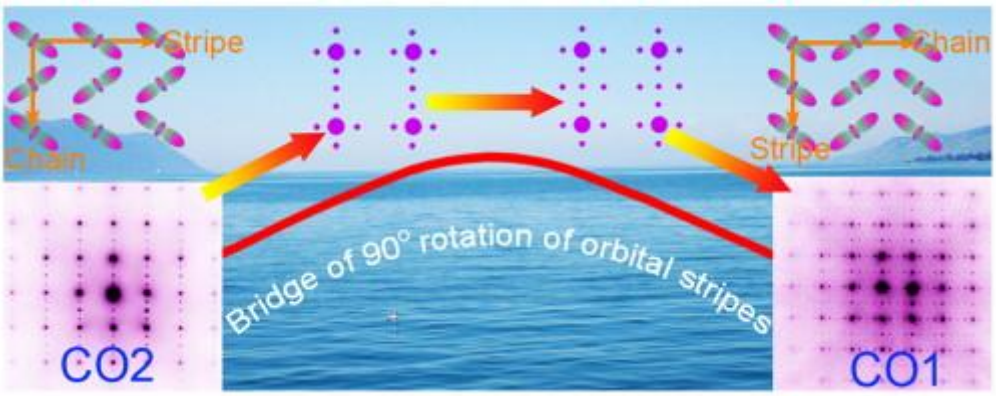

Highlights

► Intermediate states to bridge the 90° rotation of the orbital stripes in bilayer manganite $PrCa_2Mn_2O_7$ were identified. ► Some restricted conditions for the orbital rotation to occur were found and reasons were discussed. ► The reported CO2 phase at high temperatures in $PrCa_2Mn_2O_7$ can also exist at room temperature.

Stability, electronic structures and transport properties of armchair (10, 10) BN/C nanotubes

Original Research Article
Pages 294-298
H.P. Xiao, Chaoyu He, C.X. Zhang, L.Z. Sun, Pan Zhou, Jianxin Zhong

Graphical abstract

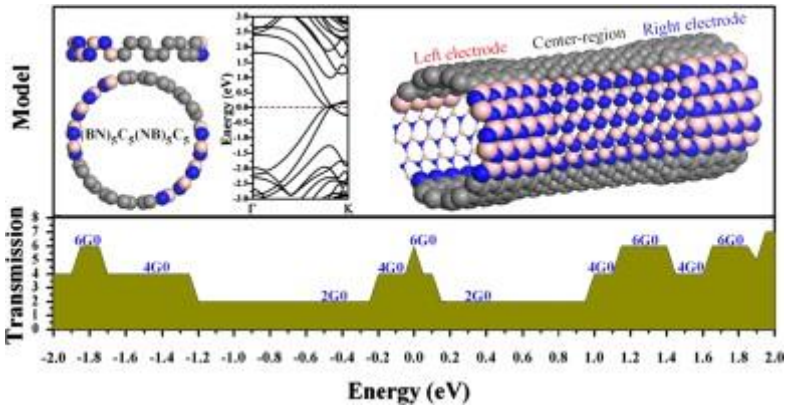

Highlights

► Transport properties of two types of four-segment BNC hybrid nanotubes are studied. ► Transport enhancements are realized in the four-segment BNC hybrid nanotubes. ► Electron and hole separation is found in four-segment BNC hybrid nanotubes.

Design of half-metallic properties induced by 2*p* impurities in ZnO nanosheet

Original Research Article
Pages 299-304
Fu-bao Zheng, Chang-wen Zhang, Hang-xing Luan, Sheng-shi Li, Pei-ji Wang

Graphical abstract

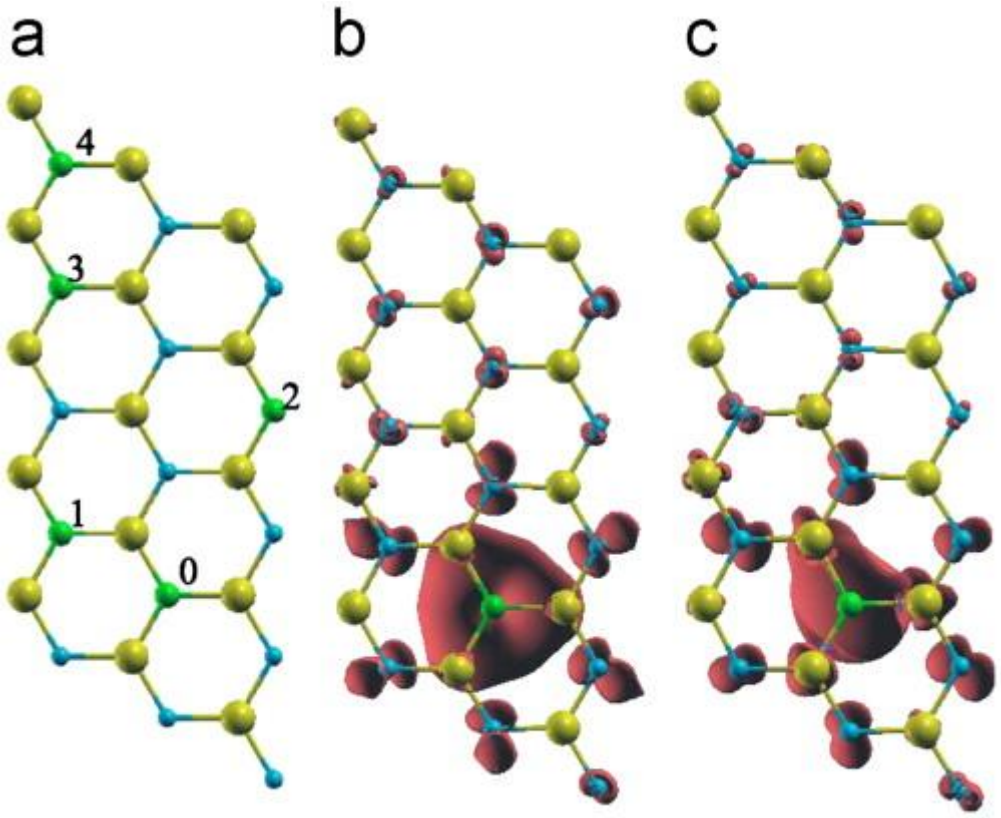

Highlights

► *X*-induced spin polarizations result in half-metallicity. ► The local moments equal to unpaired electrons in 2*p* spin states of *X* atom. ► The FM, AFM, and NM states are all found in *X*-doped ZnONSs. ► The half-metallicity in C and N doped cases are robust.

Mechanical relaxation in thermoelectric oxide $Ca_{3-x}Sr_xCo_4O_{9+\delta}$ (x=0, 0.25, 0.5, 1.0) associated with oxygen vacancies

Original Research Article
Pages 305-309
H. Liu, G.C. Lin, X.D. Ding, J.X. Zhang

Graphical abstract

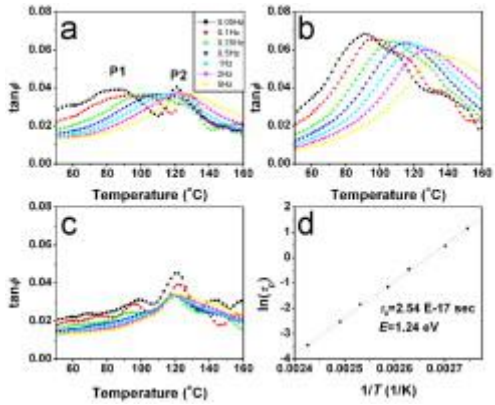

Highlights

► We performed dynamic mechanical analysis on the thermoelectric oxide $Ca_3Co_4O_{9+\delta}$. ► We observed a relaxation peak and a transition peak. ► The oxygen vacancies are located in CoO layer of Ca_2CoO_3 subsystem. ► The relaxation peak originates from migration of single oxygen vacancies.

Phase stabilisation of hexagonal barium titanate doped with transition metals: A computational study

Original Research Article
Pages 310-316
J.A. Dawson, C.L. Freeman, J.H. Harding, D.C. Sinclair

Graphical abstract

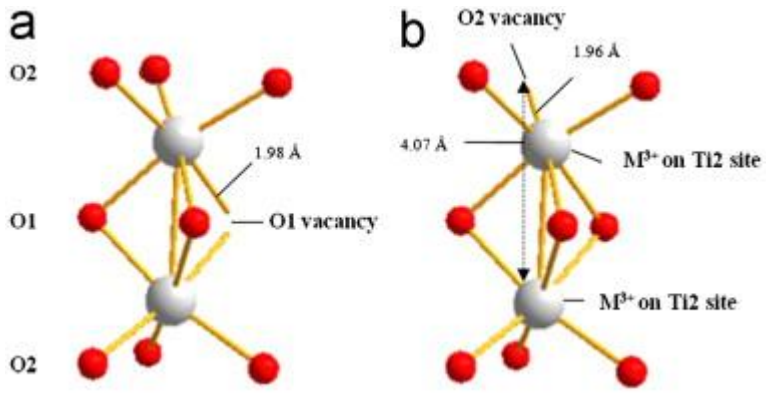

Highlights

► Classical simulations show a significant energetic gain when doping occurs at Ti sites in the face sharing dimers (Ti2 sites) of the hexagonal polymorph compared with the doping of the

cubic polymorph. ► This energetic difference between the two polymorphs is true for all transition metals tested and all charge states. ► In the case of tri- and tetra- valent dopants negative solution energies are found for the hexagonal polymorph suggesting actual polymorph stabilisation occurs with the incorporation of these ions.

Low temperature synthesis, photoluminescence, magnetic properties of the transition metal doped wurtzite ZnS nanowires

Original Research Article
Pages 317-322
Jian Cao, Donglai Han, Bingji Wang, Lin Fan, Hao Fu, Maobin Wei, Bo Feng, Xiaoyan Liu, Jinghai Yang

graphical abstract

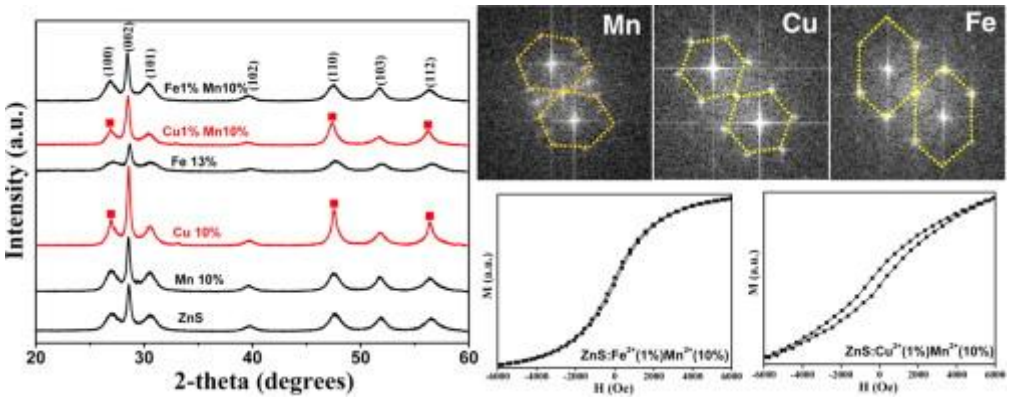

Highlights

► The transition metal ions doped wurtzite ZnS nanowires were synthesized at 180 °C. ► There was no phase transformation from hexagonal to cubic even in a large quantity introduced for all the samples. ► The room temperature ferromagnetism properties of the co-doped nanowires were investigated.

$BiNb_3O_9$, a metastable perovskite phase with Bi/vacancy ordering: Crystal structure and dielectric properties

Original Research Article
Pages 323-327
William G. Mumme, Ian E. Grey, Bryce Edwards, Christopher Turner, Juan Nino, Terrell A. Vanderah

Graphical abstract

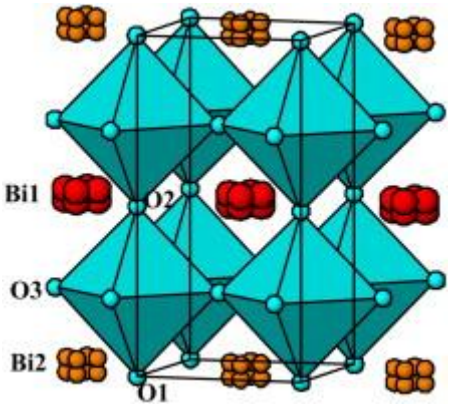

Highlights

► First characterisation of a new perovskite phase with potentially useful dielectric properties.

► Solving of the structure using single crystal data on a multiply twinned crystal. ► Measurement of dielectric properties that show the phase has a high dielectric permittivity.

Investigation of a new willemite-type compound, $(Li, Na, H)_{0.16}Zn_{1.92}SiO_4$

Original Research Article
Pages 328-340
S.-H. Park, C.J. Chucholowski, L.Garcia B. Lara, M. Hoelzel, C. Paulmann

Graphical abstract

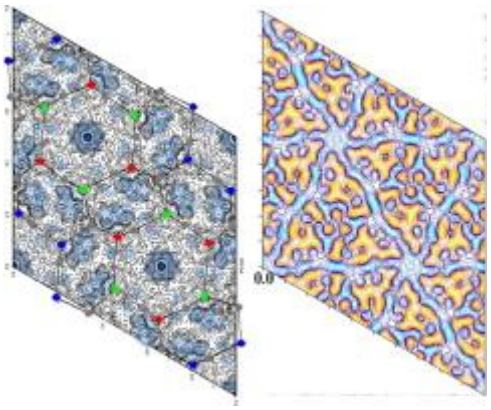

Highlights

► A new willemite-type compound, $(Li, Na, H)_{0.16}Zn_{1.92}SiO_4$ could be found for the first time.

► X-ray and neutron diffraction studies indicate the presence of Li^+, Na^+, and H^+. ► The

presence of these channel cations is attributed to 4% vacancy at Zn sites. ► This material can be regarded as a prototype for combined cationic conductors.

Inorganic polymers from alkali activation of metakaolin: Effect of setting and curing on structure

Original Research Article
Pages 341-348
Isabella Lancellotti, Michelina Catauro, Chiara Ponzoni, Flavia Bollino, Cristina Leonelli

Graphical abstract

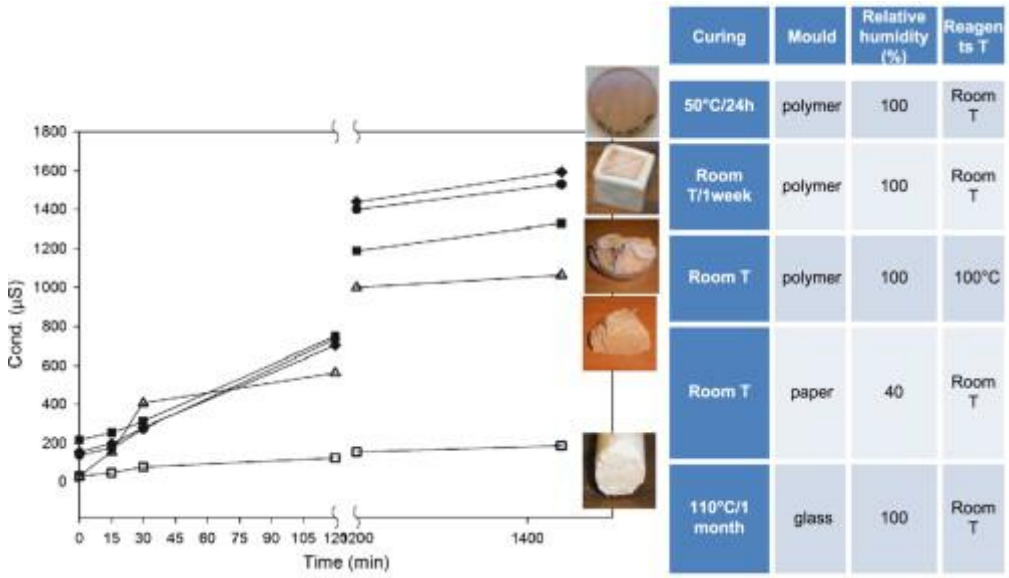

Highlights

► Metakaolin in highly alkaline solutions produced solid materials at room temperature. ► Curing time and temperature, relative humidity, reagents temperature were optimized. ► Leaching tests were used to confirm final hardening. ► FTIR spectroscopy, SEM analysis and X-ray diffractometry were used to interpret matrix stability.

Synthesis, crystal structure, and optical properties of $Ba_2Cu_2ThS_5$, and electronic structures of $Ba_2Cu_2ThS_5$ and $Ba_2Cu_2US_5$

Original Research Article
Pages 349-353
Adel Mesbah, Sébastien Lebègue, Jordan M. Klingsporn, Wojciech Stojko, Richard P. Van Duyne, James A. Ibers

Graphical abstract

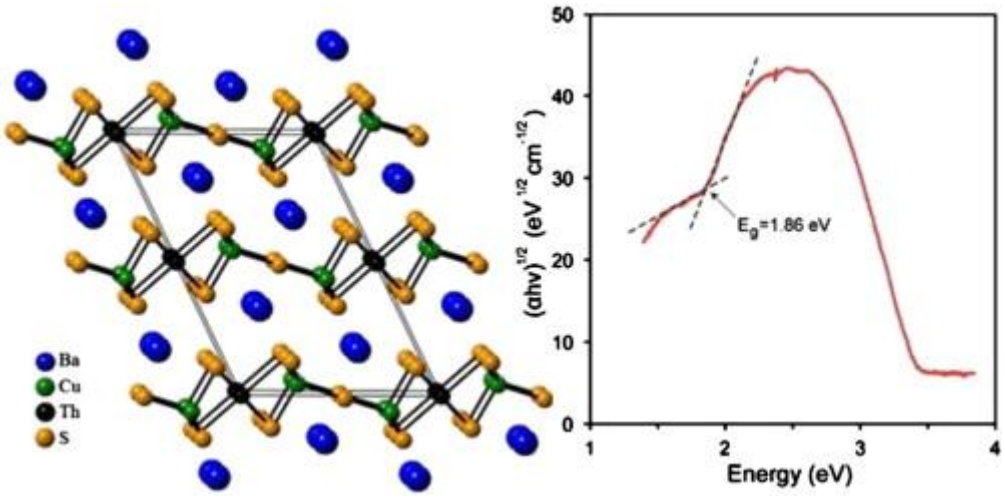

Highlights

► The new solid-state compound $Ba_2Cu_2ThS_5$ has been synthesized from BaS, S, Cu, and Th at 1173 K. ► Single-crystal optical measurements indicate of indirect band gap of 1.86 eV for $Ba_2Cu_2ThS_5$. ► DFT with the HSE06 functional predict band gaps of 1.7 and 1.5 eV for $Ba_2Cu_2ThS_5$ and $Ba_2Cu_2US_5$.

Effects of A-site composition and oxygen nonstoichiometry on the thermodynamic stability of compounds in the Ba–Sr–Co–Fe–O system

Original Research Article
Pages 354-362
Speranta Tanasescu, Zhèn Yáng, Julia Martynczuk, Vera Varazashvili, Florentina Maxim, Florina Teodorescu, Alina Botea, Nicolae Totir, Ludwig J. Gauckler

Graphical abstract

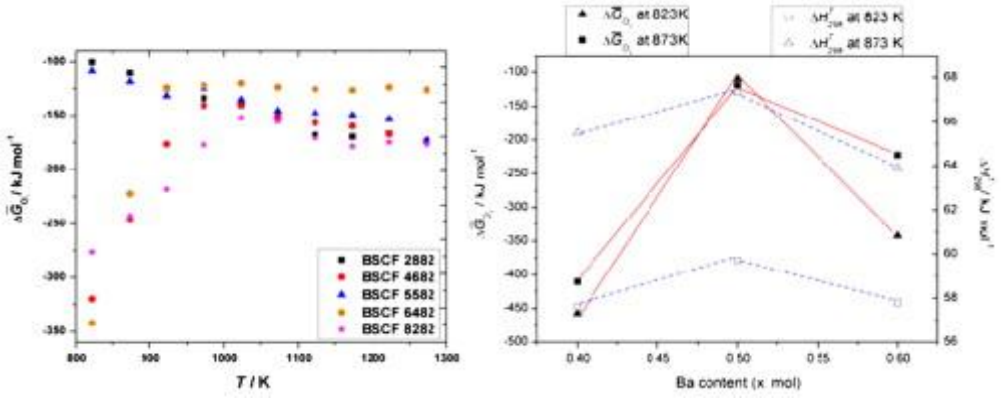

Highlights

► We report relevant data for thermodynamic stability of $Ba_xSr_{1-x}Co_{1-y}Fe_yO_{3-\delta}$ compounds. ► Temperature of structural transformations is evidenced as a function of Ba content. ► Correlation between thermodynamic, electrical and structural data is investigated. ► The results are discussed based on the properties-defect structure relationship.